

Detailed design for additive manufacturing and post processing of generatively designed high tibial osteotomy fixation plates

Kanagalingam, Sanjeevan; Dalton, Chris; Champneys, Peter; Boutefnouchet, Tarek; Fernandez-Vicente, Miguel; Shepherd, Duncan E. T.; Wimpenny, David; Thomas-Seale, Lauren E. J.

DOI:

[10.1007/s40964-022-00342-2](https://doi.org/10.1007/s40964-022-00342-2)

License:

Creative Commons: Attribution (CC BY)

Document Version

Publisher's PDF, also known as Version of record

Citation for published version (Harvard):

Kanagalingam, S, Dalton, C, Champneys, P, Boutefnouchet, T, Fernandez-Vicente, M, Shepherd, DET, Wimpenny, D & Thomas-Seale, LEJ 2022, 'Detailed design for additive manufacturing and post processing of generatively designed high tibial osteotomy fixation plates', *Progress in Additive Manufacturing*.
<https://doi.org/10.1007/s40964-022-00342-2>

[Link to publication on Research at Birmingham portal](#)

General rights

Unless a licence is specified above, all rights (including copyright and moral rights) in this document are retained by the authors and/or the copyright holders. The express permission of the copyright holder must be obtained for any use of this material other than for purposes permitted by law.

- Users may freely distribute the URL that is used to identify this publication.
- Users may download and/or print one copy of the publication from the University of Birmingham research portal for the purpose of private study or non-commercial research.
- User may use extracts from the document in line with the concept of 'fair dealing' under the Copyright, Designs and Patents Act 1988 (?)
- Users may not further distribute the material nor use it for the purposes of commercial gain.

Where a licence is displayed above, please note the terms and conditions of the licence govern your use of this document.

When citing, please reference the published version.

Take down policy

While the University of Birmingham exercises care and attention in making items available there are rare occasions when an item has been uploaded in error or has been deemed to be commercially or otherwise sensitive.

If you believe that this is the case for this document, please contact UBIRA@lists.bham.ac.uk providing details and we will remove access to the work immediately and investigate.



Detailed design for additive manufacturing and post processing of generatively designed high tibial osteotomy fixation plates

Sanjeevan Kanagalingam¹ · Chris Dalton² · Peter Champneys³ · Tarek Boutefnouchet⁴ · Miguel Fernandez-Vicente² · Duncan E. T. Shepherd¹ · David Wimpenny² · Lauren E. J. Thomas-Seale¹

Received: 19 April 2022 / Accepted: 26 August 2022
© The Author(s) 2022

Abstract

Integration of advanced technologies have revitalised treatment methods in the current clinical practice. In orthopaedic surgery, patient-specific implants have leveraged the design freedom offered by additive manufacturing (AM) exploiting the capabilities within powder bed fusion processes. Furthermore, generative design (GD), a design exploration tool based on the artificial intelligence, can integrate manufacturing constraints in the concept development phase, consequently bridging the gap between AM design and manufacturing. However, the reproducibility of implant prototypes are severely constrained due to uncomprehensive information on manufacturing and post processing techniques in the detailed design phase. This paper explores the manufacturing feasibility of novel GD concept plate designs for High Tibial Osteotomy (HTO), a joint preserving surgery for a patient diagnosed with osteoarthritis in the knee. A design for AM (DfAM) workflow for a generatively designed HTO plate is presented, including; detailed DfAM of GD concept designs, fabrication of plate prototypes using electron beam powder bed fusion (PBF-EB) of medical grade Ti-6Al-4 V, post processing and inspection. The study established PBF-EB as a suitable manufacturing method for the highly complex GD plate fixations, through evaluating the impact of manufacturing and post processing on the surface finish and geometrical precision of the plate design features.

Keywords Additive manufacturing · Generative design · High tibial osteotomy · Fixation plate · Electron beam powder bed fusion · Mass finishing

1 Introduction

To date, additive manufacturing (AM) has had a transformational impact on clinical practice; including surgical simulation, drug delivery systems, medical devices, personalised

and cost-effective care [1–3]. The orthopaedic industry has pioneered the use of AM, through precise preoperative planning, visualisation [4], intraoperative navigation, patient-specific surgical instrumentation and implants, enabling the reduction in operating times whilst improving safety,

✉ Sanjeevan Kanagalingam
sxx153@student.bham.ac.uk

Chris Dalton
Chris.Dalton@the-mtc.org

Peter Champneys
peter.champneys@autodesk.com

Tarek Boutefnouchet
tboutefnouchet@hotmail.com

Miguel Fernandez-Vicente
Miguel.Fernandez-Vicente@the-mtc.org

Duncan E. T. Shepherd
D.E.Shepherd@bham.ac.uk

David Wimpenny
David.Wimpenny@the-mtc.org

Lauren E. J. Thomas-Seale
L.E.J.Thomas-Seale@bham.ac.uk

¹ Department of Mechanical Engineering, School of Engineering, University of Birmingham, Birmingham, UK

² The Manufacturing Technology Centre, Ansty Park, Coventry, UK

³ Autodesk Technology Centre, Small Heath Business Park, Birmingham, UK

⁴ University Hospitals Birmingham NHS Trust, Birmingham, UK

accuracy and reproducibility of outcomes, even for minimally invasive surgery [5, 6]. Additive manufactured metallic implants are extensively used in joint replacements [7], fracture fixations [8], corrective osteotomies [9], and bone tumour surgery [10]. Recently, artificial intelligence (AI) has seen an explosive growth within the healthcare setting in diagnosis generation, therapy selection and risk predictions, thus aiding the clinical decision-making process [11, 12].

Osteoarthritis (OA) is a major source of chronic pain and disability, affecting approximately 15% of the world population [13]. High Tibial Osteotomy (HTO) is a joint preserving surgery for OA in the knee, offloading the mechanically overloaded compartment, to relieve pain and optimise joint movement [14, 15]. HTO necessitates osteosynthesis (fixation of bone), using metallic plates to internally fixate and stabilise the joint, allowing the patient to engage in daily activities [16]. Despite evidence of good long-term outcomes [17], the ‘one-size-fits-all’ approach in HTO has limited its surgical adoption [18, 19], primarily due to size and rigidity of the plates [20, 21]. Patient-specific AM devices have begun to address the limitations of ‘one-size-fits-all’ approach in HTO [22]. Patient specificity offers anatomically congruent fixation, minimising the size and stiffness disparity and improving mechanobiological performance [23]. More recently, Tilton et al. [8] demonstrated an AM-centric workflow for the design and development of patient-specific plate fixations. However, Burton et al. [24] highlight a distinct lack of information in academic literature on the design and manufacturing process of AM implants. This emanates from lack of expert knowledge in clinical specialisms, specific manufacturing techniques and the commercial sensitivity associated with some proprietary methods [24].

This research will present novel concept designs generated by the first application of Generative Design (GD) to HTO fixation. This paper will outline the detailed design requirements of these HTO plates for manufacturing by Powder Bed Fusion Electron Beam (PBF-EB) AM technology, including the post-processing steps required to transform the digital design into a physical part.

1.1 Background

Although AM has exposed the limitations of the current computer-aided design (CAD) systems, the recent integration of tools, such as topology optimisation (TO) and GD have expanded the capability of AM and enhanced design freedom, enabling the fabrication of strong, light-weight structures with complex organic shapes [25]. GD is a designer driven design exploration process based on AI [26], which utilises algorithms in conjunction with application-specific knowledge, to co-create a range of design solutions [27, 28]. The manufacturing intelligence embedded within the GD technology bridges the known deficits in knowledge

between AM design and manufacturing [29, 30]. Briard et al. [31] outlines a framework to maximise the potential of AM in the automotive industry. They propose a GD for AM (G-DfAM) methodology comprising four successive phases: translation, initialisation, AM guidelines integration and refinement.

A traditional metal AM implant process chain includes; 3D visualisation of anatomy, surgical planning, implant design, build preparation, manufacture and post processing, with interchange between software and hardware capabilities throughout [32, 33]. Design engineers have amplified the patient specificity of implants by exploiting design for AM (DfAM) approaches, such as imaged-based personalisation, lattice structures and TO [34]. To date, application of GD for medical devices has been limited to concept designs of orthosis and prosthesis [35, 36]. Rajput et al. [36] illustrate how the translation and initialisation phase can produce concept designs for a lightweight prosthetic leg. Yet, this novelty also leads to a lack of knowledge regarding detailed design, build preparation, manufacture, and post processing to progress a GD concept design through to a physical part.

Ti-6Al-4 V, a commonly used biomaterial for metallic implants [37], can be processed by powder bed fusion technique via both laser and electron beam (PBF-LB and PBF-EB) methods [38]. Although similar in operation to PBF-LB, PBF-EB uses an electron beam for the melting and fusion of the powder particles, with the entire process taking place in a vacuum chamber [39, 40]. The case study by Cronskär et al. [41] demonstrates the commercial viability of PBF-EB to produce personalised Ti-6Al-4 V implants, reporting a 35% cost reduction as compared to conventional machining. The application of TO for plate fixations and their fabrication using PBF-EB has been studied previously [42]. PBF-EB manufactured Ti-6Al-4 V plates have been reported to be mechanically superior compared to commercially available plates, however, it was also highlighted that post processing is essential to yield a smooth part that can minimise friction between the plate and surrounding soft tissue [43]. Mass finishing and sandblasting are prevalent abrasive industrial techniques used to manipulate surface roughness of implants [44, 45].

Up until now, HTO surgical procedures have specifically exploited AM in the form of personalised assistive technologies, in three-dimensional surgical planning [46] and as patient-specific surgical guides [47] to address the need for accuracy in planning and execution [48–50]. Recently, TOKA® (Tailored Osteotomy for Knee Alignment), established a personalised surgical treatment for HTO [51], using titanium plate fixations produced by PBF-LB, incorporating geometric patient-specific design [52].

Unlike conventionally designed HTO plates [53], in this study, the application of GD has allowed concept designs to be undertaken simultaneously considering patient factors,

surgical planning parameters and patient-specific biomechanics with the aim to reduce plate stiffness and profile on soft tissue. To date, no academic literature has investigated the design space between GD concepts and physical parts. This paper will focus on the detailed DfAM process and post processing of two GD HTO fixation concept designs. The workflow of the study includes: (1) the detailed design process in progressing a concept GD to a manufacturable design; (2) PBF-EB manufacture of HTO plates followed by post processing; and (3) the optical inspection of physical prototypes at different stages of the manufacture and post processing.

2 Materials and methods

2.1 Overview

Two AM conceptual designs were extracted from the GD process applied to HTO plates. Nine prototypes of each conceptual design, altogether eighteen plates were manufactured and post processed in this study. A summary of the workflow is shown in Fig. 1, incorporating; detailed DfAM, definition of the build parameters for PBF-EB, post processing using

mass finishing and CNC machining to create the hole and thread features. PBF-EB and mass finishing of the plates were completed at the Manufacturing Technology Centre, CNC machining was undertaken at the Autodesk Technology Centre. The resulting geometric and surface build quality were analysed. Due to cost and time constraints, only one sample of each plate was assessed ($n = 1$).

2.2 Conceptual designs of HTO plates from generative design

GD [Fusion360, Autodesk, San Rafael, California, United States] imposes geometric constraints during concept development by defining the material and method of manufacture [26]. A detailed description on GD process can be found in the literature [30]. In this study, AM was selected to process Ti-6Al-4 V alloy, with respect to an overhang angle constraint of 45 degrees and a wall thickness of 3 mm. Two designs, corresponding to two different build directions, were extracted (Fig. 2). Organic forms represented by T-NURCC (Non-Uniform Rational Catmull-Clark surfaces with T-junctions) surfaces were combined with input solid geometries via an automated Boolean operation within Fusion360, resulting in a boundary representation (B-rep)

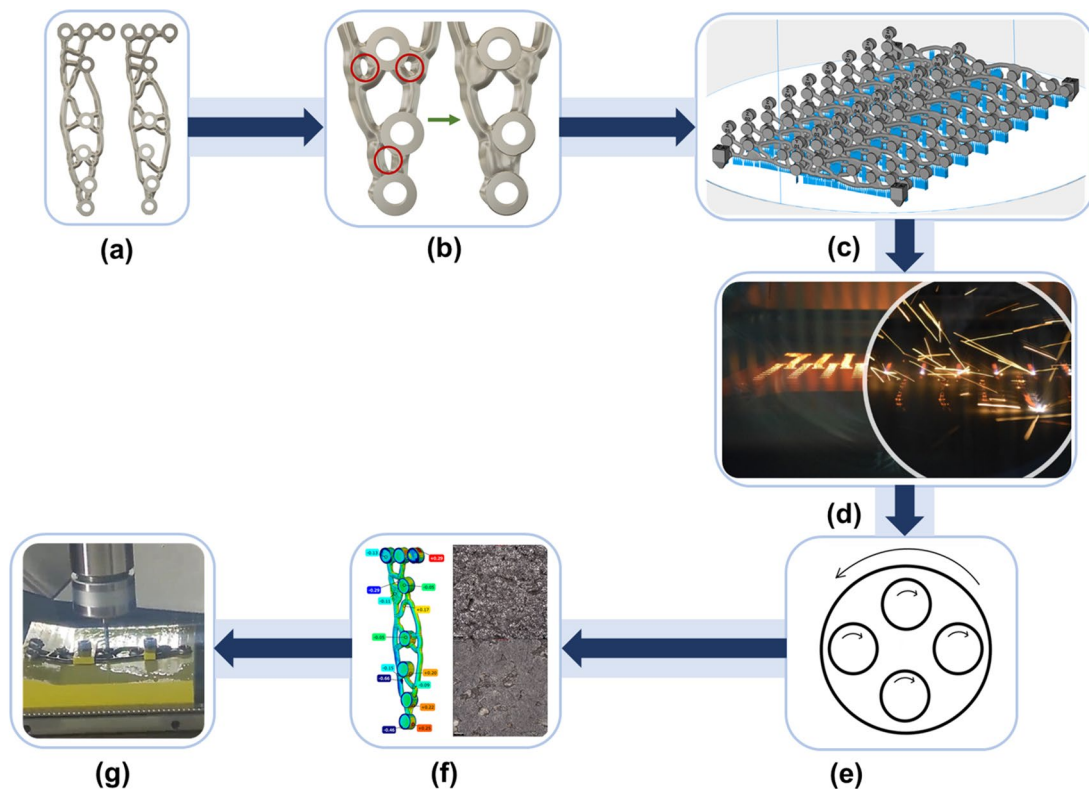
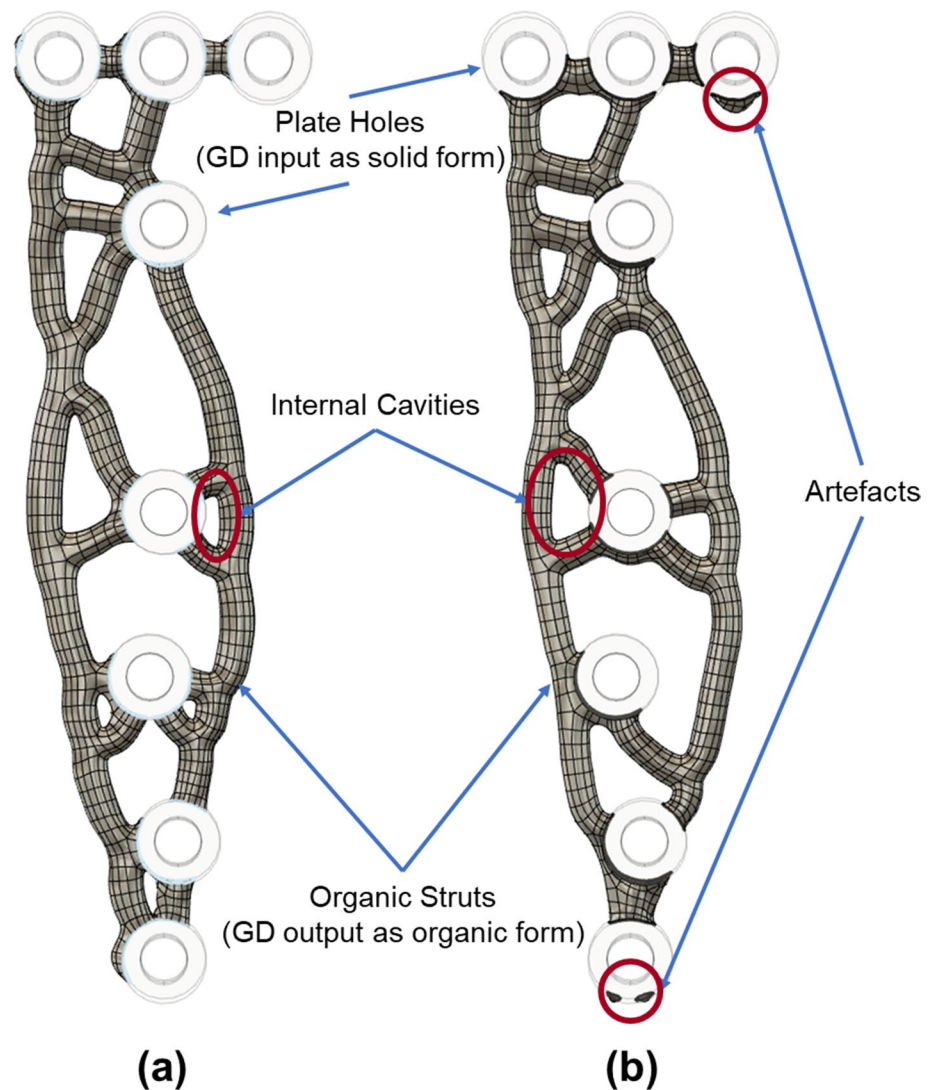


Fig. 1 G-DfAM workflow for HTO plate fixations, **a** GD HTO plate conceptual designs, **b** design optimisation of GD plate conceptual designs, **c** PBF-EB build preparation, **d** PBF-EB manufacture of Ti-

6Al-4 V plates, **e** mass finishing, **f** optical surface inspection, **g** CNC machining of plate holes and threads

Fig. 2 Organic form of HTO conceptual designs from GD, **a** plate A, **b** plate B



and thus a unified solid geometry of the concept plates [54]. Traces of organic form found within the design were identified as artefacts.

2.3 Design optimisation

3D solid geometries (IGES format) of the concepts were imported into Netfabb Ultimate 2022 software (Autodesk, San Rafael, California, United States) for further analysis. Dimensional analysis of the plate designs identified geometrical features that required modification to conform with the requirements of PBF-EB, mass finishing and CNC machining. Plate designs were modified using a combination of parametric and T-spline modelling within Fusion360.

Internal cavities were modified by editing the organic form. The cavities were closed by selecting the internal faces and using the erase and fill tool (Fig. 3a). Subsequently, adjacent vertices in the resulting concave surface

were pinched using the weld vertices tool, reducing the depth, and adding material (Fig. 3b). The smoothing operation was performed iteratively, reducing the curvature of the form surface (Fig. 3c), until the cavity was completely filled (Fig. 3d). Artefacts were isolated and removed from the design. Threads in the plate holes, were to be manufactured using CNC machining (post-AM), hence stock was added to create a flat surface, referred as plate pads (Fig. 3e). Additional stock was incorporated on the plate pads (Fig. 3f) and globally across the plate geometry to account for material loss due to post processing. Fillets were added to interfaces between the organic form and input solids, along with the edges of the plate holes, to alleviate sharp discontinuities (Fig. 3g, h).

2.4 Build preparation

Optimised designs were converted into STL format and then integrated into a manufacturing file for the ARCAM

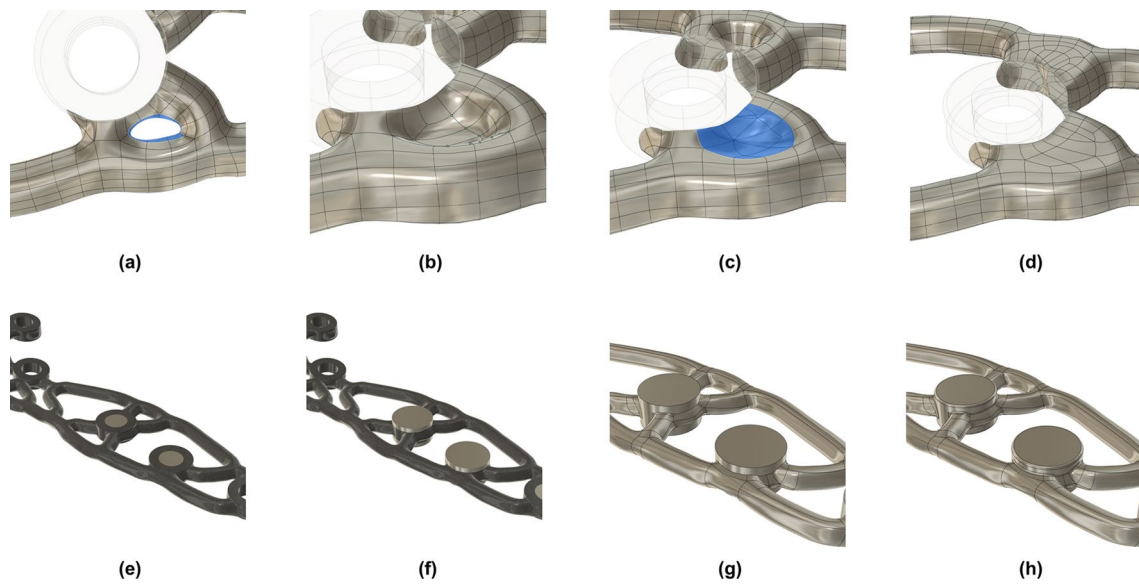


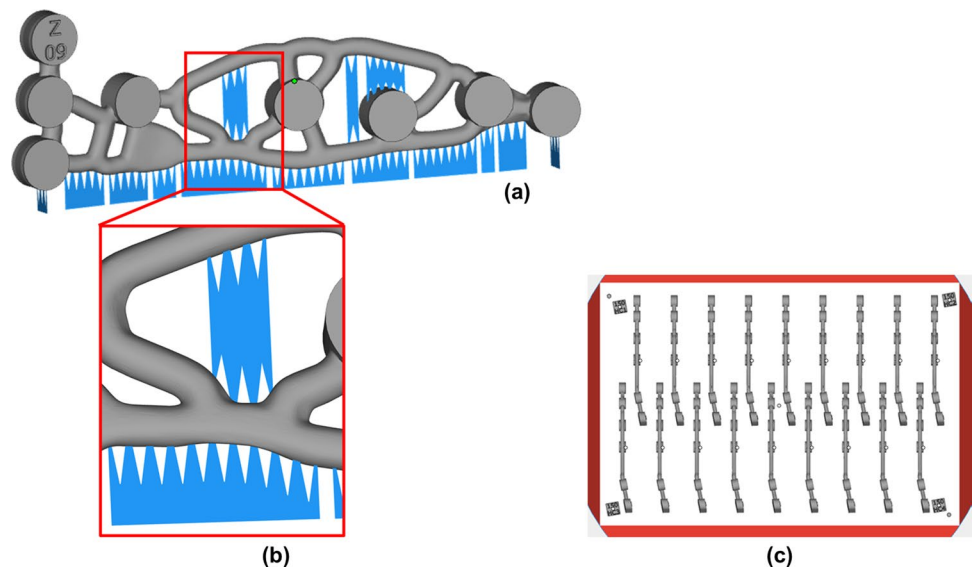
Fig. 3 Optimisation of design features in GD HTO conceptual plates, **a** face selection to erase and fill, **b** selection of vertices to weld, **c** iterative smoothing over area, **d** closed cavity, **e** modifying plate holes

to create plate pads, **f** stock addition on plate pads, **g** sharp edges and discontinuity in the organic form, **h** fillet addition

EBM Q20 plus (GE ADDITIVE, General Electric, Boston, Massachusetts, United States) using MAGICS (Materialise, Leuven, Belgium) software. Plates were oriented in the virtual build volume with ~ 3.5 mm offset from the build plate (Fig. 4a). Parts were labelled on the face of a plate pad for identification. To compensate for warping/shrinkage, parts were scaled with 1.0092, 1.0092, and 1.0132 in x, y, and z build directions, respectively. Supports were generated to achieve minimum possible attachments whilst maintaining confidence in the build success. Parts were primarily supported on the two plate pads and the struts, across the length

of the plate (Fig. 4b). Teeth-shaped connections were used for the ease of support removal. 9 replicas of each design were generated, capitalising the build area, packing a total of 18 plates in an alternating manner within the build platform (Fig. 4c). Density cubes were included in the build to ensure quality control of part porosity. Subsequently, all parts were sliced using the ARCAM EBM Q20 plus machine process parameters (Sect. 2.5) to produce an ARCAM Build Processor (ABP) file for the manufacture.

Fig. 4 PBF-EB build preparation in MAGICS, **a** part orientation, **b** teeth shaped support connections, **c** build nesting



2.5 Electron beam powder bed fusion and post processing

All implants were manufactured using GE Additive Grade 23 Ti-6Al-4 V feedstock, with powder size distribution of 45–106 μm . The ARCAM EBM Q20 plus process features a thermionic emission gun, which uses a tungsten filament operating at 60 kV to produce an electron beam. Standard GE Additive process themes were applied (version 5.2.24). A substrate plate (300×220 mm) made of stainless steel was used, preheated to ~495 °C, with the build chamber maintained at approximately 650–750 °C throughout the process. The powder was selectively melted with a layer thickness of 0.09 mm. For the hatch process, the maximum current was 28 mA, with line offset of 0.22 mm. The process took place in a vacuum at $\sim 4 \times 10^{-3}$ mbar in the chamber and $\sim 1.2 \times 10^{-6}$ mbar in the gun.

Following manufacture, a GE Additive Powder Recovery Station (PRS) was used to remove all trapped powder through blasting a stream of high-pressure air. The parts were detached from the build plate and then the support structures were removed using pliers. Thereafter, parts were sand blasted using the Guyson Euroblast 4 (Guyson International Ltd, Skipton, United Kingdom) cabinet with Saftigrit White (grade 80/90) as blasting media.

2.6 Mass finishing

Centrifugal high energy finishing (CHEF) was used to finish the components, using the CPM10 system (ActOn, Coventry, United Kingdom). The finishing was performed in three stages as shown in (Table 1). Process parameters used in this study were adopted from those used on Ti-6Al-4 V AM components [55]. Angle-cut triangular-shaped ceramic media were used in both the cutting and smoothing stages, whilst granulated Maizorb was used for polishing, with fresh media being used at the start of each process (Fig. 5). The multistage process was completed under wet and dry (wet usually includes the addition of water and brightening chemicals to the media) conditions.

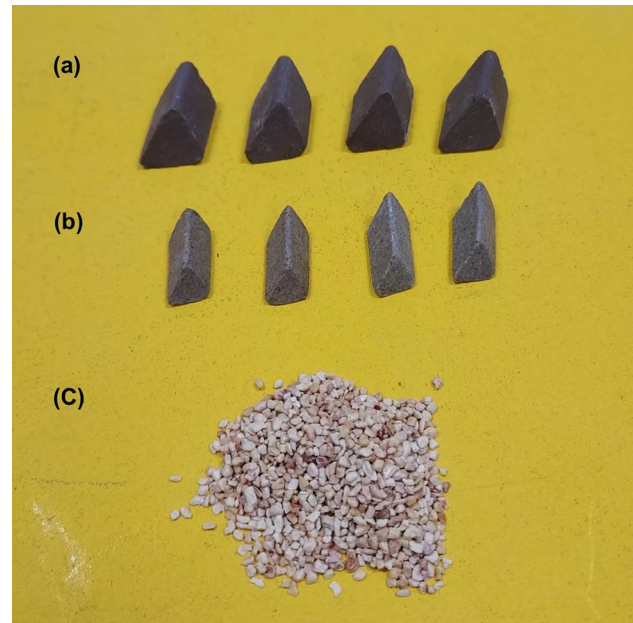


Fig. 5 Abrasive media used in the CHEF process, **a** SFB 10×10, **b** CFB 6×10, **c** Pre-treated Maizorb

2.7 Surface inspection

2.7.1 Optical microscopy and surface roughness measurement

A three-dimensional optical profiler instrument was used to assess the morphology of the implant surface after manufacture (as-built) and after the CHEF process (polished). Surface roughness measurements were obtained by visualising the surface through confocal laser scanning microscopy using the Sensofar S Neox (SENSOFAR METROLOGY, Barcelona, Spain) equipped with a 10× objective lens. A combination of flat and curved surfaces (Table 2) across distinctive regions (Fig. 6) of plate A and B were evaluated. The bottom surface of as-built parts were not examined due to anchored supports in the region (Fig. 6a). Both flat faces of the plate pad (Fig. 6c, d), and the closed cavity within plate A were profiled (Fig. 6b). The scans were imported to MountainMaps Premium 8.1 (Digital Surf, Besançon, France) software for analysis. Both the arithmetic average of the surface roughness, R_a , and the average arithmetic height

Table 1 CHEF process parameters

Stage	Media	Compound	Time (mins)	Material removal rate
Cutting	SFB 10×10	50 ml LQ18 + water	120	High
Smoothing	CFB 6×10	50 ml LQ16 + water	120	Medium
Polishing	Pre-treated Maizorb	None (dry)	60	Low

Table 2 Surface area corresponding to scan region of plate surfaces

Plate surface scan region	Scan area (mm x mm)
Bottom (B)	5.0×1.4
Top (T)	5.0×1.4
Closed cavity (CC)	5.5×3.5
Plate Pad 1 (P1)	4.7×5.3
Plate Pad 2 (P2)	4.7×5.3

of the surface, S_a , were reported according to ISO 4287 and ISO 25178, respectively.

2.7.2 3D scanning and geometric deviations of surface

Geometrical surface accuracy was compared between the optimised digital design (part build geometry from MAG-ICS), to the physical part (post-CHEF). The scan of the physical parts were obtained using the ATOS III Triple Scan (GOM, Braunschweig, Germany). The comparisons were taken from STL files, in which the geometries generated in the build preparation stage were used as reference. Thereafter, STL representation of the physical parts were aligned using the global best-fit algorithm. Upon aligning, the surface normal deviations between selected surfaces were analysed using GOM 2021 (GOM, Braunschweig, Germany).

2.8 Machining

The holes and threads were machined using the DMG Mori (DMG Mori Aktiengesellschaft, Bielefeld, Germany) DMU 60 eVo 5 axis milling machine. STL files of both plate

designs (optimised designs) were used to plan the machining strategy, defining machining operations and process parameters, to produce a custom G-code for DMU 60 eVo (Fusion360). Resin based fixturing (Fig. 7) was employed to mount the workpiece in order to avoid surface impingement of the polished AM parts.

3 Results and discussion

3.1 Generative design outcomes for HTO plates

The GD outcomes for HTO plates are shown in (Fig. 8). In contrast to conventional plate fixations [53], GD produced a network of organic looking struts, branching and interconnecting the predefined plate holes throughout the macro-geometry. Based on the plate-hole configuration, the digital plates had the same proximal-to-distal length and same anterior-to-posterior width; 104 and 31 mm, respectively.

The design freedom offered by PBF-EB can leverage the geometric opportunities of GD. However, whilst AM constraints were imposed early on in the GD process, it did not account for post processing of the final part, essential for future clinical application. The designs from GD required further analysis and modification to accommodate DfAM requirements and attain a manufacturable design. The organic nature coupled with the specified design constraint (minimising plate stiffness) produced pockets of internal cavities across the plate. As seen in Fig. 3g, the interfaces between the organic form and input solids, as well as the edges of the plate holes, revealed sharp discontinuities in the design. Minor artefacts were found in both plates.

Fig. 6 Scan regions of plates for optical microscopy, **a** bottom and top curved surfaces **b** closed cavity of plate A, **c** plate pad 1, **d** plate pad 2

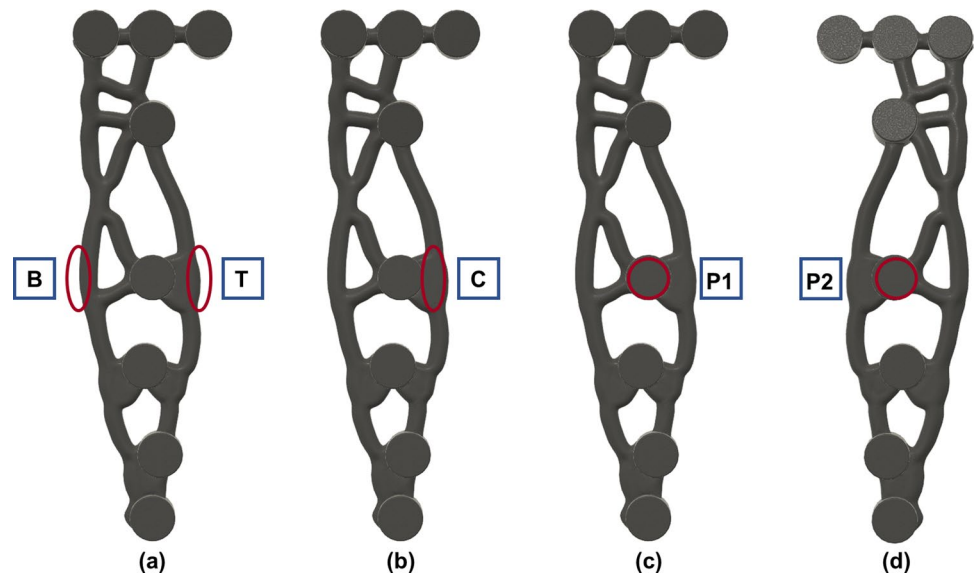


Fig. 7 Custom resin fixturing machined with negatives of plate design **a** plate A, **b** plate B

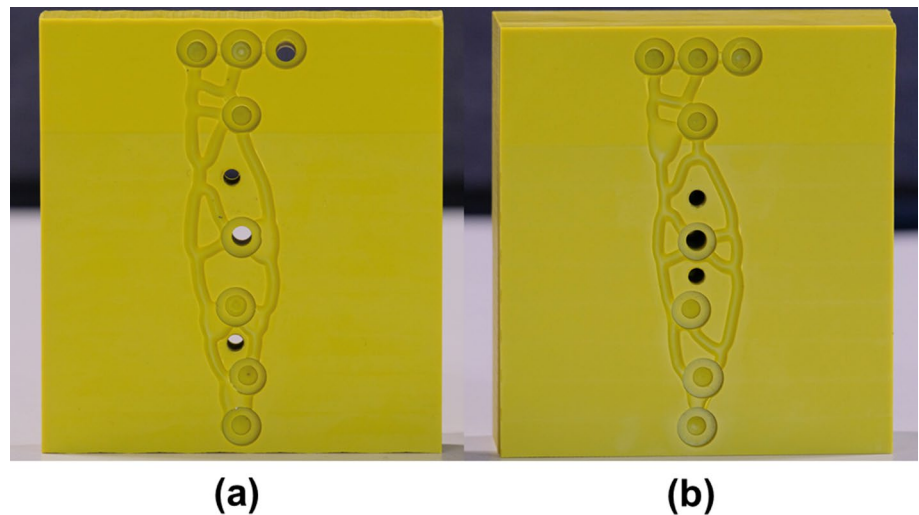
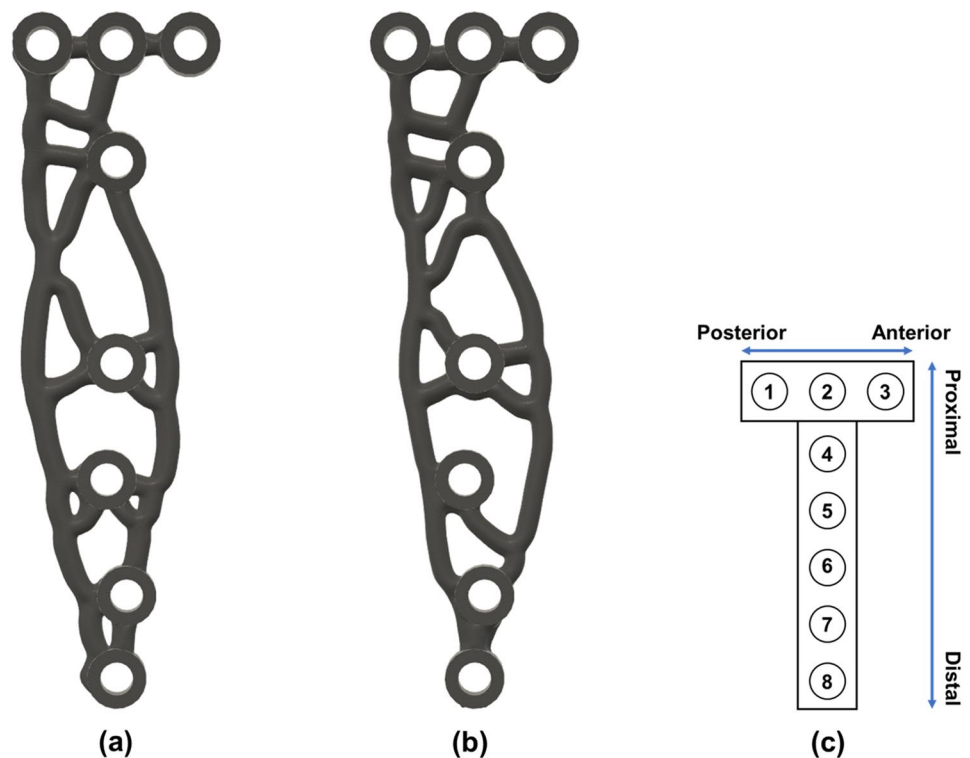


Fig. 8 GD concepts for HTO plate design, **a** plate A, **b** plate B, **c** plate-screw configuration



3.1.1 Geometric analysis of optimised GD HTO plates

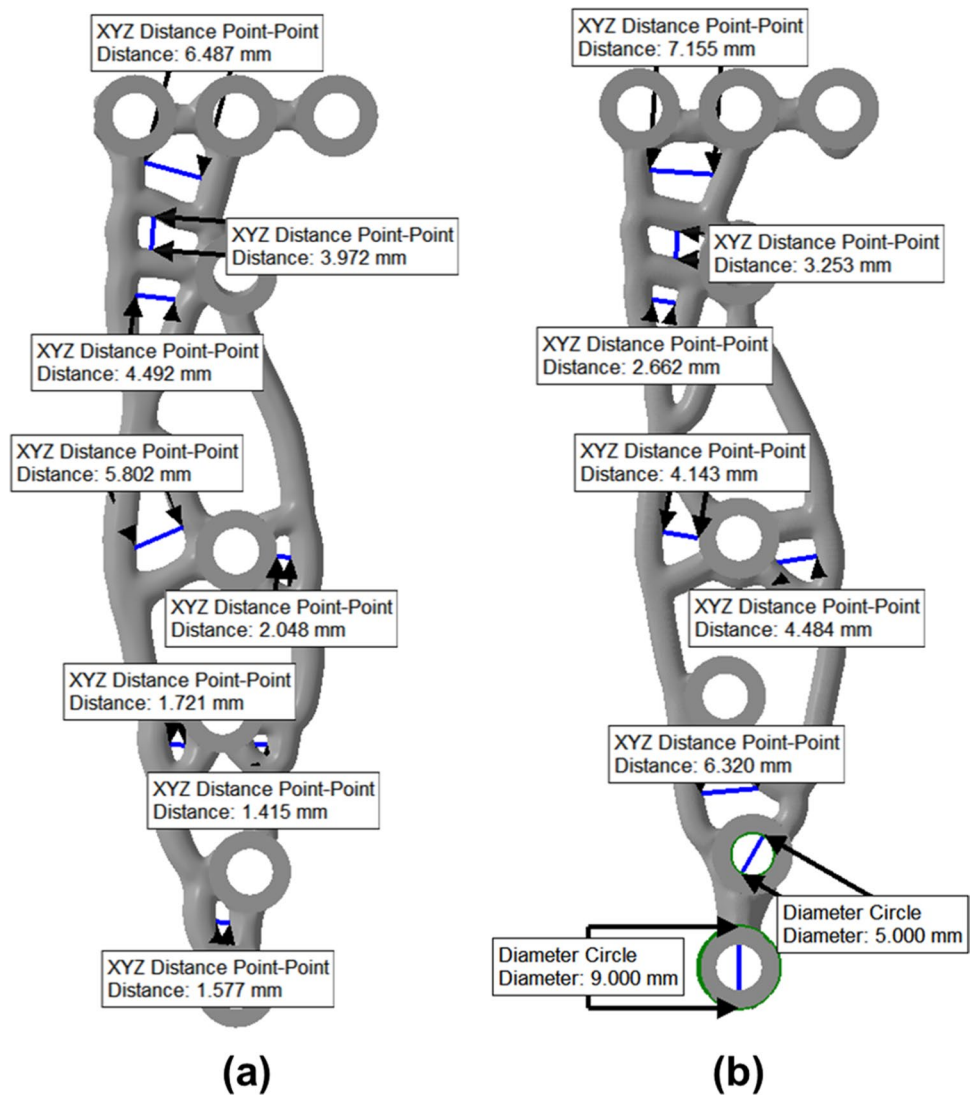
A standard part analysis confirmed both designs were made up of a single shell fully enclosed solid (i.e., neither design contained holes, degenerated faces or inverted triangles), attesting the watertightness of the IGES. Dimensional analysis of the digital plates are shown in (Fig. 9). All plate holes had an inner and outer diameter of 5 and 9 mm, respectively. Internal cavity features were digitally measured point-to-point across their largest cross section and were found to be ranging from 1.4 to 7.1 mm in both designs. Internal cavities

with a cross section below 3 mm were considered to be inaccessible by the abrasive media that was used in the CHEF post process and therefore required further modifications.

3.1.2 Design modifications of GD HTO plates

As shown in Fig. 10, four cavities in plate A and one in plate B were filled with material using T-spline modelling (Sect. 2.3) to avoid inhomogeneous post processing around the internal curved regions of the cavity. To account for post processing, all plate holes across both designs were filled

Fig. 9 Dimensional analysis of the design features in GD HTO conceptual plates, **a** plate A, **b** plate B



with material, creating plate pads. Stock was added to the plates; 0.5 mm globally, compensating for removal of material during CHEF and 1 mm on either side of the plate pads, leaving adequate stock for machining holes. Sharp edges and continuities were modified using fillets, and therefore removing potential stress concentrations within the design (Fig. 11).

3.2 Manufactured HTO plates

The total build time for the designed plates using the PBF-EB process was 10 h 8 min, comprising pre-heating of build platform (1 h 15 min), processing (6 h 50 min) and cool down (2 h 2 min). An as-built density of 99.66% was

characterised using the density cubes. Following the removal of excess powder, the plates remained attached to the build platform (Fig. 12). Upon support removal, one prototype of each design, were treated with abrasive media using sand-blasting and then the CHEF process. The progression of HTO plates from as-built through to a polished surface finish is shown in (Fig. 13).

3.2.1 Surface roughness (As-built vs Polished)

The surface evaluation between post-PBF-EB and post-CHEF provides the arithmetic average of the surface roughness (R_a) and the average arithmetic height of the surface (S_a) (Table 3). Example scans from plate A, comparing the

Fig. 10 Design optimisation of inaccessible internal cavities, **a** plate A, **b** plate B

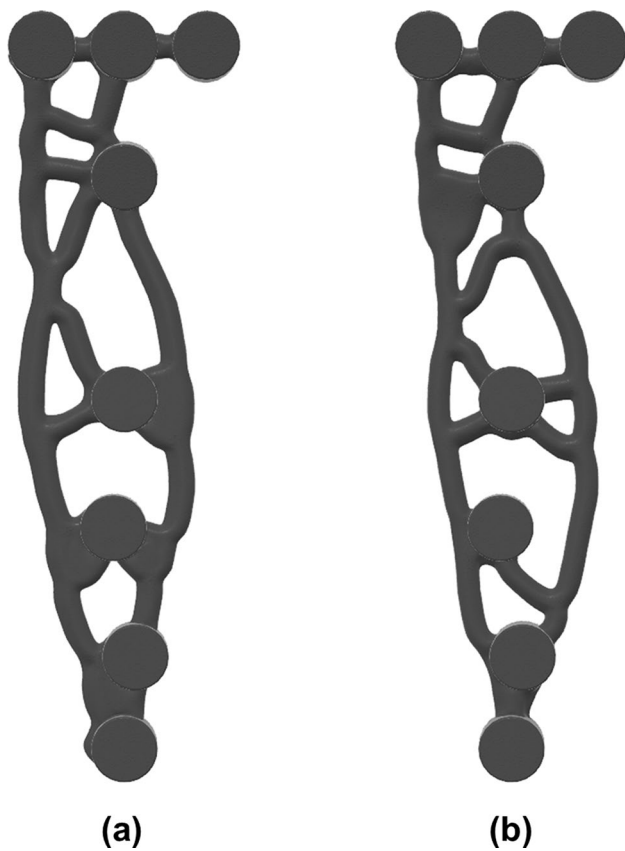
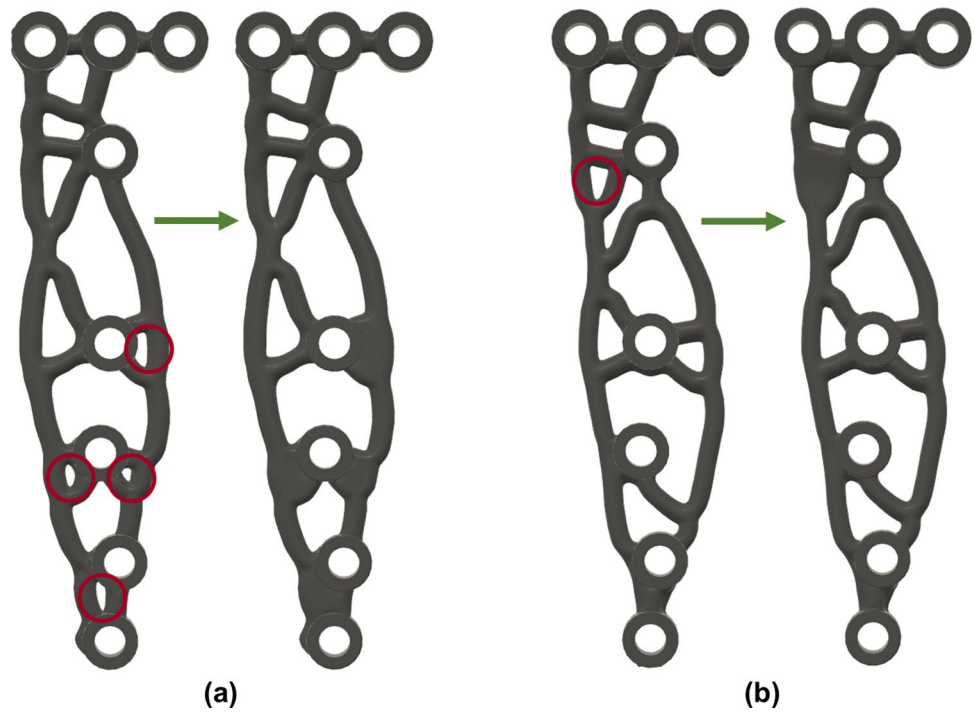


Fig. 11 Optimised GD HTO conceptual plates, **a** plate A, **b** plate B

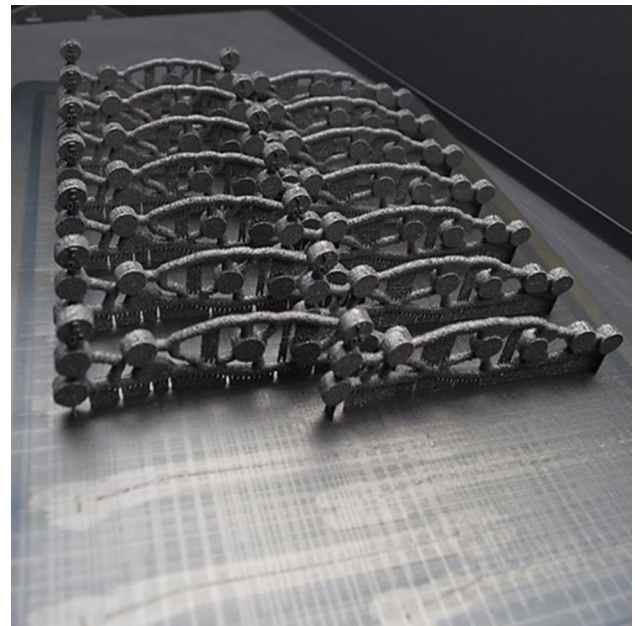


Fig. 12 As-built Ti-6Al-4v HTO plates attached to build platform

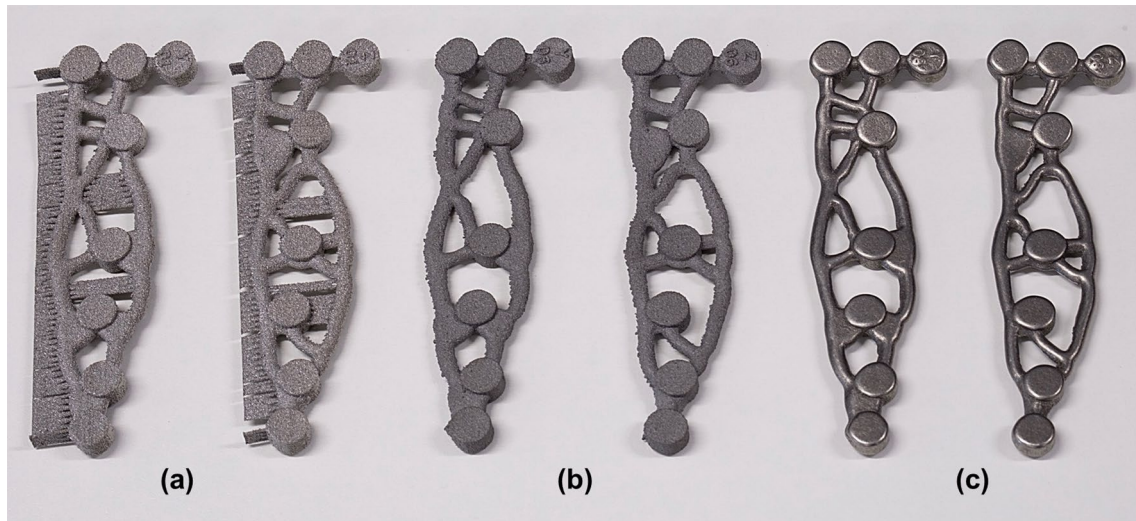


Fig. 13 PBF-EB manufactured Ti-6Al-4v HTO plate prototypes at different stages of post processing, **a** As-built with trailing supports, **b** post-sand blasting, **c** post-CHEF

surface topology (3D and 2D) between as-built and polished prototypes for both flat and curved regions are shown in Figs. 14, 15, respectively.

The as-built plates processed by PBF-EB had initial R_a and S_a roughness ranging between 22.89–33.68 and

15.14–30.61 μm , respectively. The process parameters used in PBF-EB and the powder particle size influence the surface roughness of parts [42, 43]. The surface roughness values of the as-built GD HTO plates are higher in comparison to those reported for R_a $0.49 \pm 0.02 \mu\text{m}$ of a PBF-EB clavicle

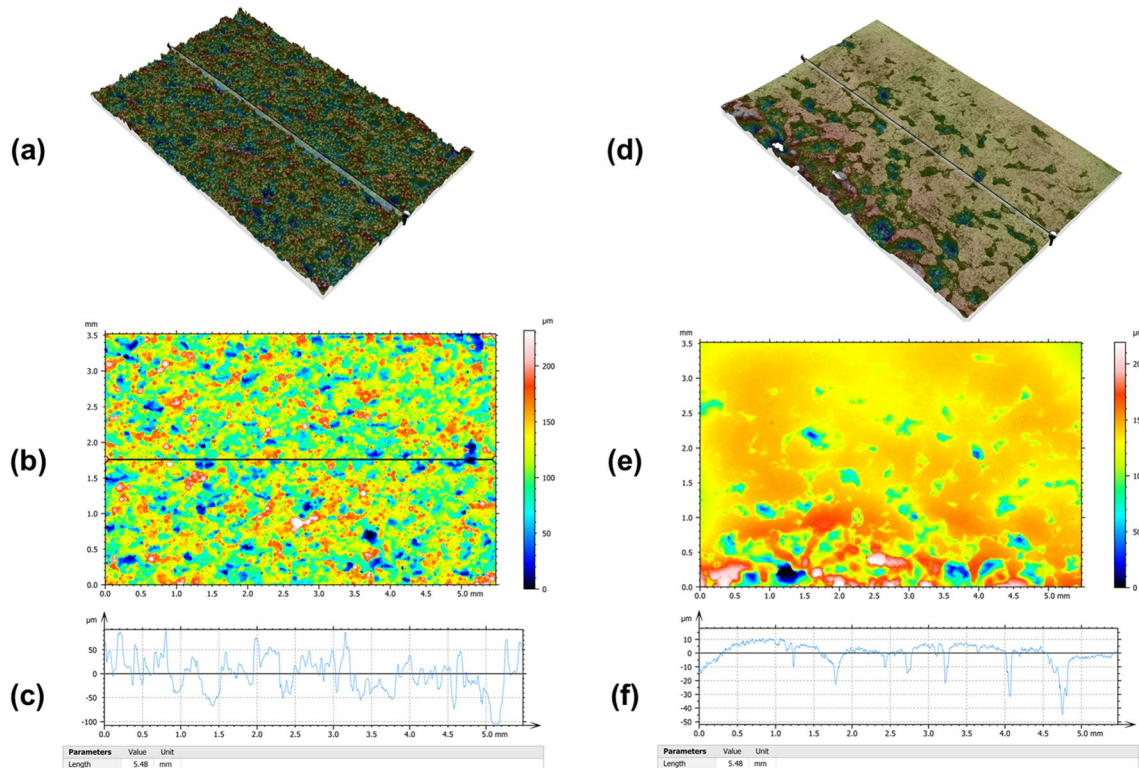


Fig. 14 Roughness comparison of the closed cavity (C) scan region in plate A, **a** 3D surface of the as-built closed cavity, **b** 2D surface roughness height across the scan area of as-built closed cavity **c** surface roughness height across the line of as-built closed cavity, **d** 3D

surface of the polished closed cavity, **e** 2D surface roughness height across the scan area of polished closed cavity, **f** surface roughness height across the line of polished closed cavity

	Scan Region				Plate A				Plate B			
	As-built		Polished		% Difference		As-built		Polished		% Difference	
	R_a (μm)	S_a (μm)	R_a (μm)	S_a (μm)	R_a (μm) (%)	S_a (μm) (%)	R_a (μm)	S_a (μm)	R_a (μm)	S_a (μm)	R_a (μm) (%)	S_a (μm) (%)
B	-	-	1.46	0.78	-	-	-	-	1.74	0.85	-	-
T	22.89	15.14	1.06	0.77	95.4	94.9	24.63	15.14	1.08	0.85	95.6	94.4
CCC	25.85	20.40	9.71	3.12	62.4	84.7	-	-	-	-	-	-
P1	29.97	26.28	4.57	7.15	84.8	72.8	30.97	24.15	5.83	9.59	81.2	60.3
P2	33.31	23.62	3.48	3.98	89.6	83.1	33.68	30.61	3.52	1.94	89.5	93.7

plate $0.49 \pm 0.02 \text{ }\mu\text{m}$ [43] and S_a of $12.42 \pm 1.11 \text{ }\mu\text{m}$ for an as-built PBF-EB plate [42]. In these studies, the macrogeometries of the plates are contained within one plane, as opposed to complex 3D geometries seen in this study. However, further research would be required to confirm causation. The abrasive media used in CHEF process decreased the surface roughness, both R_a and S_a , at all measurement points including flat and curved surfaces. The R_a and S_a roughness of the polished HTO plates ranged between $1.06\text{--}9.71$ and $0.77\text{--}9.59 \text{ }\mu\text{m}$ respectively. This is a significant reduction in roughness, and an important result, as it indicates that friction would be reduced between plate and surrounding soft tissue. However, these feasibility results cannot be validated through literature comparison. Cosma et al. [44] used a combination of sandblasting, carborundum polishing and ultrasonication to reduce roughness (R_a) values up to $1.2 \text{ }\mu\text{m}$, albeit this was for pure titanium processed by PBF-LB.

3.2.2 Geometric deviations (Optimised Design vs Polished)

It is evident that both plate surfaces have regions with traces (positive) and loss (negative) of material as a result of the PBF-EB fabrication and CHEF processes. The maximum positive, maximum negative and mean deviations of the surfaces in both plates are summarised in (Table 4). Sharma et al. [56] report maximum deviations of 0.55 mm for a PBF-LB manufactured biomimetic titanium plate for cranial reconstruction. The mean deviation across the overall surfaces were -0.10 and -0.11 mm, for plate A and B, respectively. This is comparable to average deviations of ± 0.12 mm in PBF-LB manufactured orthopaedic implants reported in literature [44].

Contact surfaces between the implant and support structures (Fig. 6a) create repeated regions of positive material presences, raising concerns about geometrical accuracy on the bottom surface. The areas with supports revealed positive deviations ranging between +0.22 mm and +0.63 mm, with more significant deviations in plate B compared to plate A. Cosma et al. [44] reported a maximum positive deviation of +0.48 mm on the support surfaces of a Ti-6Al-4 V knee prosthesis. Positive deviations in other regions can be found

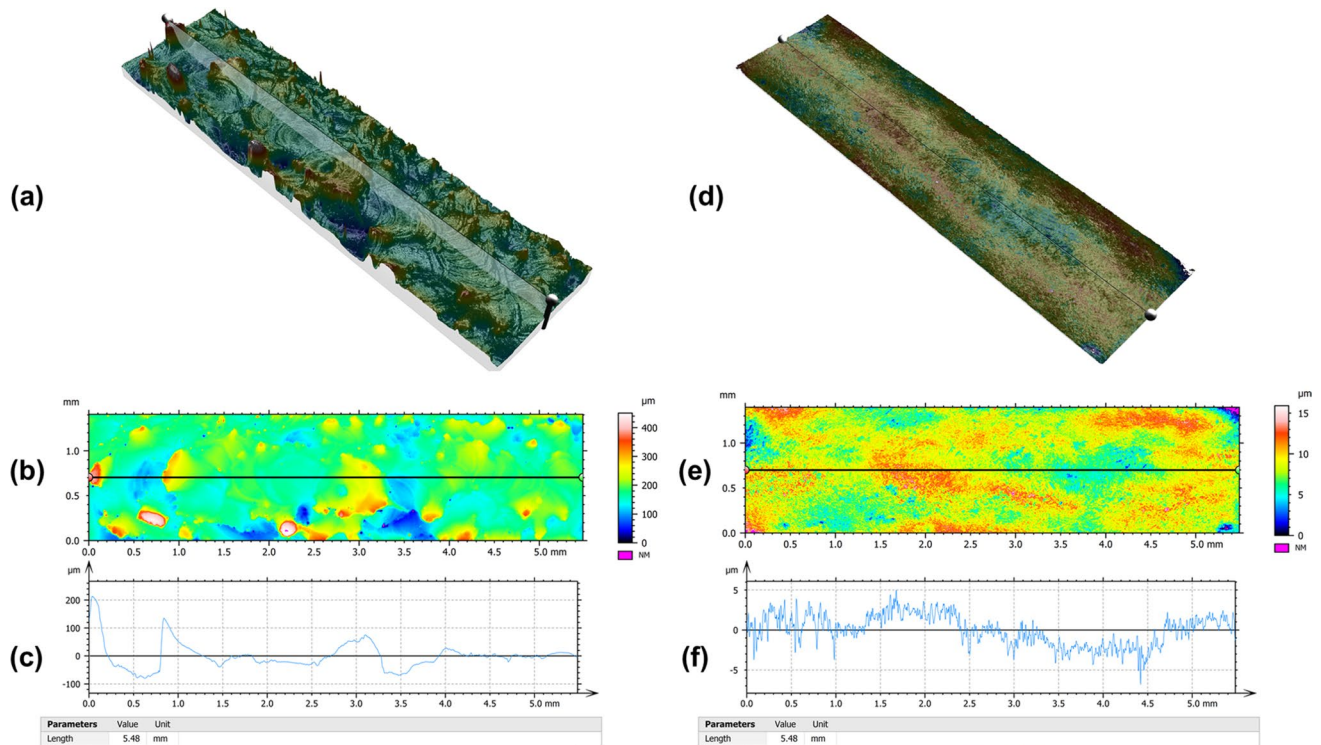


Fig. 15 Roughness comparison of the top (T) scan region in plate A, **a** 3D surface of the as-built top surface, **b** 2D surface roughness across the scan area of as-built top surface **c** surface roughness height across the line of as-built top surface, **d** 3D surface of the polished

top surface, **e** 2D surface roughness across scan area of the polished top surface, **f** surface roughness height across the line of polished top surface

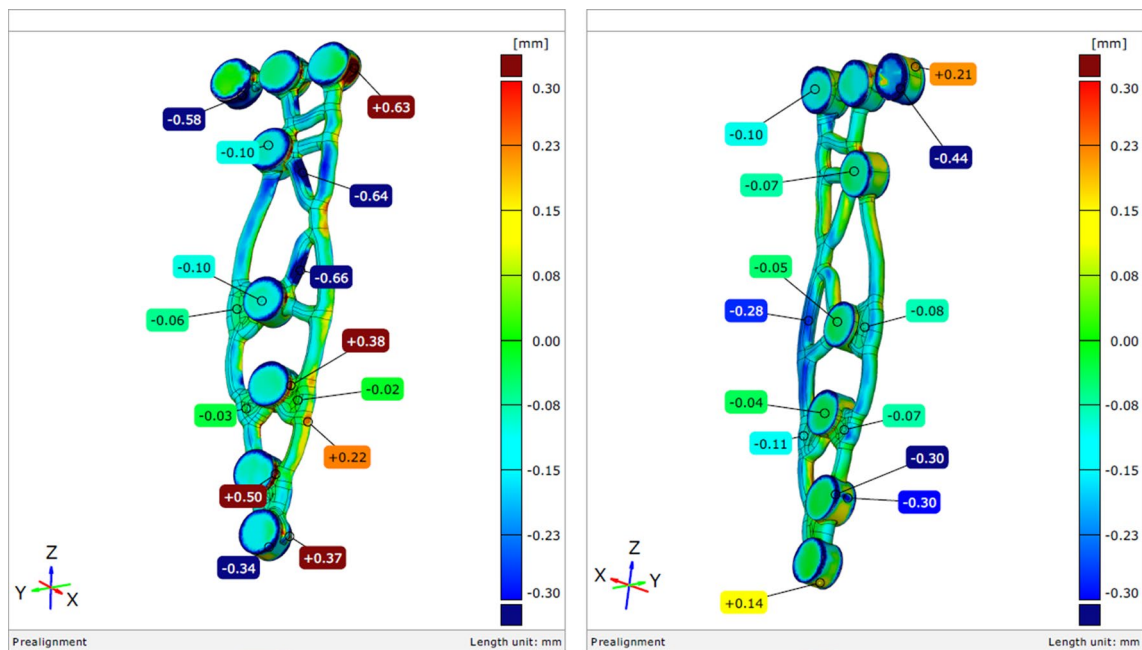


Fig. 16 Colorimetric representation of the geometric deviations in plate A

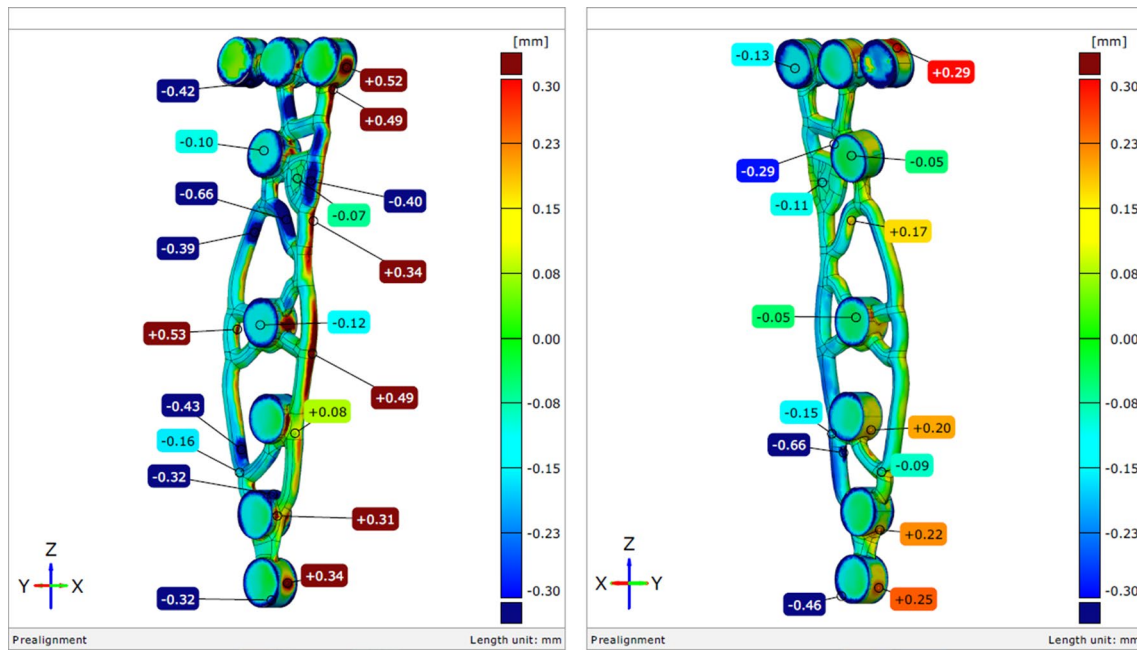


Fig. 17 Colorimetric representation of the geometric deviations in plate B

around corners of internal cavities and the interface between organic form and plate pads. This could be indicative of geometrical features that are least affected by the CHEF process. Future research is required to confirm the correlation between support and geometric features and material traces. This could be compensated for in the detailed design phase by, for example, the addition of localised as opposed to global stock.

Negative deviations were generally found around internal cavities and plate pads, ranging between -0.32 mm and -0.66 mm, across both plates. Maximum negative deviations in both plates were focussed around the internal curvature of the cavities. This could be attributed to the larger surface area offered by the curved regions of the struts to the abrasive media. In contrast, the corners of the internal cavity, especially ones with smaller corner radii, show positive deviations in the region, due to inaccessibility of media around sharp corners. In future research, increasing the internal radii of these corners may ensure more homogenous post processing of internal cavities. Alternatively, abrasive media with different shape and of relatively smaller size could be trialled. In the plate pads, flat surfaces experienced minimal loss of material ranging between -0.04 mm and -0.13 mm, this is in contrast to the rounded features, which ranged from -0.29 mm and -0.58 mm. This is hypothesised to be attributed to protruding features coming in contact with the abrasive media more often compared to the plate features.

Table 4 Geometric deviations in plate A and B

Geometric deviation	Plate A	Plate B
Maximum positive (mm)	+0.63	+0.52
Maximum negative (mm)	-0.66	-0.66
Mean (mm)	-0.10	-0.11

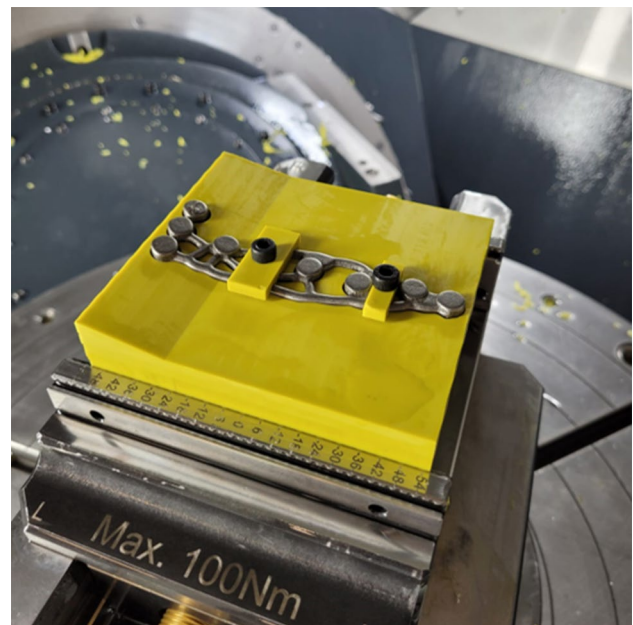
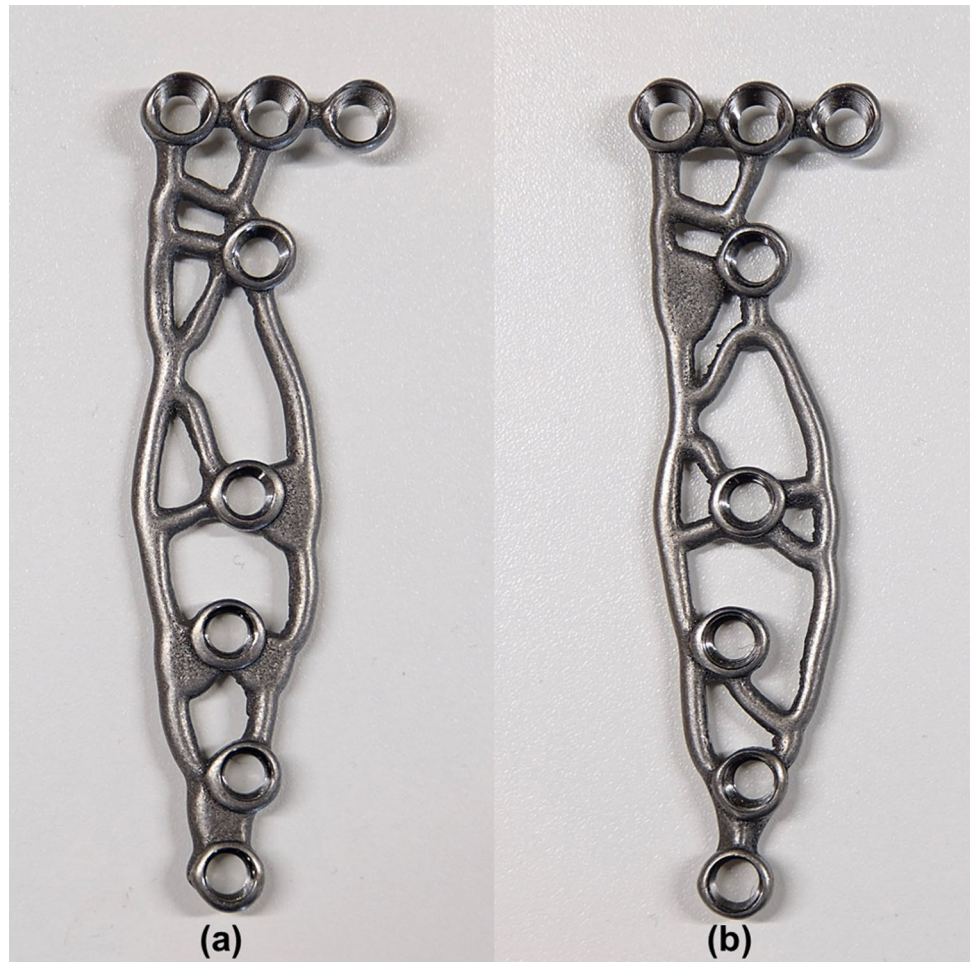


Fig. 18 Plate A clamped to the custom resin fixture for machining holes and threads

Fig. 19 GD PBF-EB manufactured Ti-6Al-4 V HTO plate prototypes (post machining), **a** plate A, **b** plate B



3.3 Machining of HTO plate holes and threads

The plates were secured to the custom fixture at two regions using the clamps and bolts as shown in (Fig. 18). All holes were machined using deep drilling and boring operations, and the internal threads were produced using a custom tool. The entire machining cycle took 1 h and 37 min. An image of the final parts can be seen in (Fig. 19).

3.4 Summary

This study explored the progression of GD concepts of HTO plates, incorporating design interventions through expert DfAM knowledge, through to PBF-EB fabrication and post processing. In this feasibility study, where sole samples of the two plate designs were assessed for surface and geometric accuracy, the results represent $n=1$. Care must be taken when generalising the numeric outcomes of this study. The comparison between the as-built surface roughness measurements of this study, and previous literature [42, 43], showed an increase in the roughness values on the comparably complex 3D geometry. However, on the different

surface contours of this study, the curved surface showed a larger reduction in surface roughness measurements after sandblasting and CHEF. The impact of manufacture and post processing on the design geometry, was also apparent in geometric deviations, relative to design features, support structures and surface curvature. Moving forward, complex features, such as the internal cavities could be finished using a combination of post processes [45] to ensure a homogenous surface finish. Future work would require repeatable intrasample and intersample studies, to ascertain statistical significance relative to feature types and samples, in line with the optimisation of the PBF-EB and post-processing parameters aligned with the detailed design modifications.

The cost was not analysed in this study. However, the advanced methods of design, fabrication, and post processing (including material, time and labour) compared to an off-the-shelf commercially available HTO T-plate, suggests a significantly higher cost per plate, as compared to the clinical standard. This is an important factor when considering commercial and clinical translation. A cost-benefit analysis of the design and manufacture of the plate compared with the long-term patient outcomes will be essential to ensure

the feasibility of clinical translation in a financially limited national health service. Considering the additive and subtractive nature of the entire process, further future research could investigate hybrid manufacturing capabilities to reduce time and cost overheads.

4 Conclusion

This research has explored the progression of G-DfAM HTO plates into manufacturable prototypes. The comprehensive workflow described detailed DfAM alterations, PBF-EB fabrication, mass finishing and further machining of the HTO plates. Surface and geometric inspections of the plates determined the impact of PBF-EB, sandblasting and the CHEF process on the original digitally defined geometry.

This study has demonstrated that PBF-EB is a viable option for the fabrication of GD HTO plates. The capability of GD to produce highly complex HTO plates, when compared to the commercial and research state of the art, was established. Although readily manufacturable with minimal design intervention, advanced analysis using CAD/CAM software was mandatory to integrate further design requirements for post processing. Whilst the finalised designs were manufacturable, the accuracy of the geometry and continuity of the surface finish correlated with design features relative to processing parameters. Future work is required to optimise process parameters of the workflow and ascertain inter and intrasample statistical significance and undertake a cost–benefit analysis. The outcomes of this study support the hypothesis that further localised design modifications, in line with post-processing parameters, could lead to higher geometric accuracy between the digital and physical part.

Acknowledgements The paper was supported by UK's Engineering and Physical Sciences Research Council (EPSRC) National Productivity Investment Fund (EP/R512436/1).

Author contributions SK: conceptualisation, methodology, data collection and analysis, writing, reviewing and editing. CD: methodology, data collection and reviewing. TB: conceptualisation and reviewing. PC: conceptualisation and reviewing. MF: supervision, conceptualisation, methodology and reviewing. DS: supervision and reviewing. DW: supervision, conceptualisation, methodology and reviewing. LTS: supervision, conceptualisation, methodology, data analysis, writing, reviewing and editing.

Declarations

Conflict of interest On behalf of all authors, the corresponding author states that there is no conflict of interest.

Open Access This article is licensed under a Creative Commons Attribution 4.0 International License, which permits use, sharing, adaptation, distribution and reproduction in any medium or format, as long

as you give appropriate credit to the original author(s) and the source, provide a link to the Creative Commons licence, and indicate if changes were made. The images or other third party material in this article are included in the article's Creative Commons licence, unless indicated otherwise in a credit line to the material. If material is not included in the article's Creative Commons licence and your intended use is not permitted by statutory regulation or exceeds the permitted use, you will need to obtain permission directly from the copyright holder. To view a copy of this licence, visit <http://creativecommons.org/licenses/by/4.0/>.

References

1. Rezvani Ghomi E, Khosravi F, Neisiany RE, Singh S, Ramakrishna S (2021) Future of additive manufacturing in healthcare. *Curr Opin Biomed Eng* 17:100255
2. Li C, Pisignano D, Zhao Y, Xue J (2020) Advances in medical applications of additive manufacturing. *Engineering* 6(11):1222–1231
3. Pugliese L et al (2018) The clinical use of 3D printing in surgery. *Updates Surg* 70(3):381–388
4. Fernandes MG, Alves JL, Fonseca EMM (2016) Diaphyseal femoral fracture: 3D biomodel and intramedullary nail created by additive manufacturing. *Int J Mater Eng Innov* 7(2):130–142
5. Javaid M, Haleem A (2018) Additive manufacturing applications in orthopaedics: a review. *J Clin Orthop Trauma* 9(3):202–206
6. Wong KC, Scheinermann P (2018) Additive manufactured metallic implants for orthopaedic applications. *Sci China Mater* 61(4):440–454
7. Narra SP, Mittwede PN, DeVincent Wolf S, Urish KL (2019) Additive manufacturing in total joint arthroplasty. *Orthop Clin N. Am* 50(1):13–20
8. Tilton M, Lewis GS, Bok Wee H, Armstrong A, Hast MW, Manogharan G (2020) Additive manufacturing of fracture fixation implants: design, material characterization, biomechanical modeling and experimentation. *Addit Manuf* 33:101137
9. Dobbe JGG, Vroemen JC, Strackee SD, Streekstra GJ (2014) Patient-specific distal radius locking plate for fixation and accurate 3D positioning in corrective osteotomy. *Strateg Trauma Limb Reconstr* 9(3):179–183
10. Ma L et al (2017) 3D printed personalized titanium plates improve clinical outcome in microwave ablation of bone tumors around the knee. *Sci Rep* 7(1):1–10
11. He J, Baxter SL, Xu J, Xu J, Zhou X, Zhang K (2019) The practical implementation of artificial intelligence technologies in medicine. *Nat Med* 25(1):30–36
12. Han X-G, Tian W (2019) Artificial intelligence in orthopedic surgery. *Chin Med J (Engl)* 132(21):2521–2523
13. Johnson VL, Hunter DJ (2014) The epidemiology of osteoarthritis. *Best Pract Res Clin Rheumatol* 28(1):5–15
14. O'Malley M, Reardon PJ, Pareek A, Krych A, Stuart MJ (2016) Opening-wedge proximal tibial osteotomy. *Arthrosc Tech* 5(4):e769–e774
15. Kolb W, Guhlmann H, Windisch C, Koller H, Grützner P, Kolb K (2010) Opening-wedge high tibial osteotomy with a locked low-profile plate: surgical technique. *J Bone Jt Surg - Ser A* 92:197–207
16. Lee DH, Ryu KJ, Kim HH, Soung S, Shin S (2015) Fixator-assisted technique enables less invasive plate osteosynthesis in medial opening-wedge high tibial osteotomy: a novel technique. *Clin Orthop Relat Res* 473(10):3133–3142

17. Floerkemeier S, Staubli AE, Schroeter S, Goldhahn S, Lobenhof P (2013) "Outcome after high tibial open-wedge osteotomy: a retrospective evaluation of 533 patients." *Knee Surgery Sport Traumatol Arthrosc* 21(1):170–180
18. Woodacre T et al (2016) Complications associated with opening wedge high tibial osteotomy - a review of the literature and of 15 years of experience. *Knee* 23(2):276–282
19. Seo S-S, Kim O-G, Seo J-H, Kim D-H, Kim Y-G, Lee I-S (2016) Complications and short-term outcomes of medial opening wedge high tibial osteotomy using a locking plate for medial osteoarthritis of the knee. *Knee Surg Relat Res* 28(4):289–296
20. Röderer G, Gebhard F, Duerksen L, Ignatius A, Claes L (2014) Delayed bone healing following high tibial osteotomy related to increased implant stiffness in locked plating. *Injury* 45(10):1648–1652
21. Pagkalos J, Hussain F, Karargyris O, Snow M (2018) A pilot study to assess the safety and radiological performance of a new low-profile locking plate for high tibial osteotomy. *Knee* 25(5):866–873
22. Jones GG, Jaere M, Clarke S, Cobb J (2018) 3D printing and high tibial osteotomy. *EFORT Open Rev* 3(5):254–259
23. Caiti G, Dobbe J, Bervoets E, Beerens M, Strackee SD, Strijkers GJ, Streekstra GJ (2019) Biomechanical considerations in the design of patient-specific fixation plates for the distal radius. *Med Biol Eng Comput* 57(5):1099–1107
24. Burton HE, Peel S, Eggbeer D (2018) Reporting fidelity in the literature for computer aided design and additive manufacture of implants and guides. *Addit Manuf* 23:362–373
25. Barbieri L, Muzzupappa M (2022) Performance-driven engineering design approaches based on generative design and topology optimization tools: a comparative study. *Appl Sci* 12(4):2106
26. McKnight M (2017) Generative design: what it is? How is it being used? Why it's a game changer. *KnE Eng* 2(2):176
27. Shea K, Aish R, Gourtovaia M (2005) Towards integrated performance-driven generative design tools. *Autom Constr* 14(2):253–264
28. Krish S (2011) Computer-aided design a practical generative design method ☆. *Comput Des* 43(1):88–100
29. Harvard Business Review Analytic Services (2018) The Next Wave of Intelligent Design Automation. Available online: <https://hbr.org/sponsored/2018/06/the-next-wave-of-intelligent-design-automation>. Accessed 31 Mar 2022
30. Leary M (2020) Generative design. *Des Addit Manuf* 2:203–222
31. Briard T, Segonds F, Zamariola N (2020) G-DfAM: a methodological proposal of generative design for additive manufacturing in the automotive industry. *Int J Interact Des Manuf* 14(3):875–886
32. Edelmann A, Dubis M, Hellmann R (2020) Selective laser melting of patient individualized osteosynthesis plates—digital to physical process chain. *Materials* 13(24):1–13
33. Tilton M, Lewis GS, Bok Wee H, Armstrong AD, Hast MW, Manogharan GP (2020) Additive manufacturing of fracture fixation implants: Design, material characterization, biomechanical modeling and experimentation. *Addit Manuf* 33:101137
34. Zadpoor AA (2017) Design for additive bio-manufacturing: from patient-specific medical devices to rationally designed meta-biomaterials. *Int J Mol Sci* 18:8
35. Ricotta V, Campbell RI, Ingrassia T, Nigrelli V (2020) A new design approach for customised medical devices realized by additive manufacturing. *Int J Interact Des Manuf* 14(4):1171–1178
36. Rajput S, Burde H, Singh US, Kajaria H, Bhagchandani RK (2021) Optimization of prosthetic leg using generative design and compliant mechanism. *Mater Today Proc* 46:8708–8715
37. Majumdar T, Eisenstein N, Frith JE, Cox SC, Biribilis N (2018) Additive manufacturing of titanium alloys for orthopedic applications: a materials science viewpoint. *Adv Eng Mater* 20:9
38. Sing SL, An J, Yeong WY, Wiria FE (2016) Laser and electron-beam powder-bed additive manufacturing of metallic implants: a review on processes, materials and designs. *J Orthop Res* 34(3):369–385
39. Körner C (2016) Additive manufacturing of metallic components by selective electron beam melting - a review. *Int Mater Rev* 61(5):361–377
40. Gokuldoss PK, Kolla S, Eckert J (2017) Additive Manufacturing Processes: Selective Laser Melting, Electron Beam Melting and Binder Jetting-Selection Guidelines. *Materials* 10(6):672
41. Cronskär M, Bäckström M, Rännar LE (2013) Production of customized hip stem prostheses - a comparison between conventional machining and electron beam melting (EBM). *Rapid Prototyp J* 19(5):365–372
42. Al-Tamimi AA, Huang B, Vyas C, Hernandez M, Peach C, Bartolo P (2019) Topology optimised metallic bone plates produced by electron beam melting: a mechanical and biological study. *Int J Adv Manuf Technol* 104(1–4):195–210
43. Liu PC et al (2014) A study on the mechanical characteristics of the EBM-printed Ti-6Al-4V LCP plates in vitro. *J Orthop Surg Res* 9:106
44. Cosma C, Balci N, Moldovan M, Morovic L, Gogola P, Miron-Borzan C (2017) Post-processing of customized implants made by laser beam melting from pure Titanium. *J Optoelectron Adv Mater* 19(11–12):738–747
45. Jamal M, Morgan MN (2017) Design process control for improved surface finish of metal additive manufactured parts of complex build geometry. *Inventions* 2(4):1–18
46. Victor J, Premanathan A (2013) Virtual 3D planning and patient specific surgical guides for osteotomies around the knee: a feasibility and proof-of-concept study. *Bone Joint J* 95-B(11 Suppl A):153–158
47. Yang JC-S et al (2018) Clinical experience using a 3D-printed patient-specific instrument for medial opening wedge high tibial osteotomy. *Biomed Res Int* 2018:1–9
48. Fucentese SF, Meier P, Jud L, Köchli GL, Aichmair A, Vlachopoulos L, Färnstahl P (2020) Accuracy of 3D-planned patient specific instrumentation in high tibial open wedge valgisation osteotomy. *J Exp Orthop* 7(1):7
49. Donnez M, Ollivier M, Munier M, Berton P, Podgorski JP, Chabrand P, Parratte S (2018) Are three-dimensional patient-specific cutting guides for open wedge high tibial osteotomy accurate? An in vitro study. *J Orthop Surg Res* 13(1):171
50. Munier M, Donnez M, Ollivier M, Flecher X, Chabrand P, Argenson J (2017) Can three-dimensional patient-specific cutting guides be used to achieve optimal correction for high tibial osteotomy? Pilot study. *Orthop Traumatol Surg Res* 103(2):245–250
51. MacLeod AR et al (2021) Personalised high tibial osteotomy has mechanical safety equivalent to generic device in a case-control in silico clinical trial. *Commun Med* 1(1):1–9
52. MacLeod AR, Serranoli G, Fregly BJ, Toms AD, Gill HS (2018) The effect of plate design, bridging span, and fracture healing on the performance of high tibial osteotomy plates: An experimental and finite element study. *Bone Joint Res* 7(12):639–649
53. Diffio Kaze A (2019) Mechanical strength of a new plate compared to six previously tested opening wedge high tibial osteotomy implants. *J Exp Orthop* 6(1):1–15
54. Marinov M et al (2019) Generative design conversion to editable and watertight boundary representation. *CAD Comput Aided Des* 115:194–205

55. Kahlin M, Ansell H, Kerwin A, Smith B, Moverare J (2021) Variable amplitude loading of additively manufactured Ti6Al4V subjected to surface post processes. *Int J Fatigue* 142:105945
56. Sharma N, Ostas D, Rotar H, Brantner P, Thieringer FM (2021) Design and additive manufacturing of a biomimetic customized cranial implant based on voronoi diagram. *Front Physiol* 12:1–12

Publisher's Note Springer Nature remains neutral with regard to jurisdictional claims in published maps and institutional affiliations.